

Giant extrinsic negative thermal expansion in vanadium pentoxide nanocrystalline films

A. A. Bahgat^{*,1,2}, A. Al-Hajry¹, and M. M. El-Desoky^{1,3}

¹ Department of Physics, Faculty of Science, King Khaled University, P.O. Box 9004, Abha, Saudi Arabia

² Department of Physics, Faculty of Science, Al-Azhar University, Nasr City 11884, Cairo, Egypt

³ Department of Physics, Faculty of Education, Suez Canal University, Al-Arish, Egypt

Received 26 September 2005, revised 9 March 2006, accepted 11 March 2006

Published online 15 May 2006

PACS 61.10.Nz, 61.46.Hk, 65.40.De, 68.55.Ln, 68.60.Dv

Vanadium pentoxide gels, $V_2O_5 \cdot 1.6H_2O$, give rise to xerogel layers that exhibit a preferred orientation. X-ray diffraction of this xerogel displays the 00 l peaks typical of a turbostratic stacking of the V_2O_5 ribbons along a direction parallel to the substrate. The distance along the c -axis is observed from the interlayer spacing to decrease continuously with increasing temperature up to 180 °C, as observed by high-temperature X-ray diffraction. This contraction may be described by an extrinsic mechanism of negative thermal expansion (NTE). The coefficient of NTE as large as $-1.5 \times 10^{-3} \text{ K}^{-1}$ was observed. Full recovery of the interlayer spacing is obtained after cooling the sample to room temperature in open air, where water molecules are reabsorbed, indicating that the process is reversible and the heating process can be repeated without losing NTE. The structure of the xerogel was explored further using differential scanning calorimetry as well as infrared spectroscopy.

© 2006 WILEY-VCH Verlag GmbH & Co. KGaA, Weinheim

1 Introduction

The vast majority of materials expand on heating – they possess a positive thermal expansion coefficient, PTE. There are, however, certain compounds, whose volumes decrease on heating, so-called NTE (negative thermal expansion) materials [1–3]. In many cases this unusual behavior can be attributed to intrinsic or extrinsic mechanisms [3, 4]. The intrinsic mechanism of the NTE phenomenon over large temperature intervals is transverse vibrations of bridging ligand atoms (e.g. oxygen) in combination with specific structural requirements, i.e. ‘space’ for the transverse vibrations, causing reduction of the metal–metal non-bonding distance. This mechanism can emerge when the material has strong metal–ligand bonds (with negligible thermal expansion) and when there is an adequate framework topology with enough internal space to allow coordinated thermal rocking of interconnected polyhedra, a consequence of transverse vibration of the bridging ligand atoms. This intrinsic mechanism was observed in ZrW_2O_8 , ZrP_2O_7 , $Y_2W_3O_{12}$, $Sc_2(WO_4)_3$, $AlPO_4$ -17, $InBi$ and in some siliceous zeolites [5–9]. Recently, on the other hand, the extrinsic mechanism of NTE was explored in ceramics with microcracks [3] and non-pure siliceous and hydrated zeolites [4, 10]. The extrinsic mechanism was explained as due to the influence of microcracks as they reclosed on reheating a ceramic substance, water dehydration, interstitial non-framework cation or molecule migration and/or dealumination [3, 4, 10]. For example, in the hydrated HZSM-5 orthorhombic zeolite, the water influence is active only at lower temperatures due to dehydration, i.e.

* Corresponding author: e-mail: alaabahgat@yahoo.com

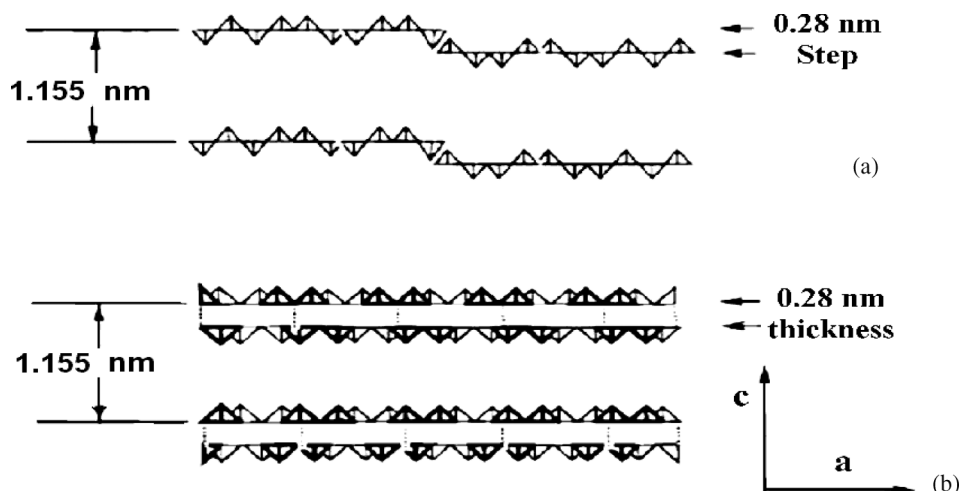


Fig. 1 Schematic picture of V_2O_5 xerogel. a) Comparison of the double-layer model according to the Livage group [21], b) the bilayer structural model according to the Oka group [22].

between 80 and 440 °C, and the NTE coefficient is $-7.38 \times 10^{-6} \text{ K}^{-1}$ [10]. However, the dealumination is expected to occur at higher temperatures (above 600 °C) in air [4, 10].

Generally, thermal expansion is one of the properties which must be considered in the application of highly functional materials, because of the mismatch of thermal expansion between component materials which can cause problems, such as mechanical destruction and positional deviation, in electrical, optical and/or high-temperature devices. One of the possible methods that can solve these problems is the control of the thermal expansion property by synthesizing a composite material showing PTE with one which shows NTE. There are applications for such materials both in the pure form and in composites to adjust the overall thermal expansion to some particular value, such as zero [11]. The discovery of materials with a negative coefficient of thermal expansion and further insights into the mechanism may therefore play an important role in theory and applications. Ranges of applications include zero-expansion heat sinks, printed circuit boards, dental applications, substrates for high-precision optical applications, low-temperature thermocouples and thermal switches, catalyst supports, cookware, etc. [12]. Excellent review articles were published giving a good background on the subject of NTE [3, 5].

On the other hand, it was recently realized that nanocrystalline materials are considered as exceptional new materials with many unexpected properties. One of the main processes of manufacturing nanocrystalline materials is the sol–gel technique [13]. This has been extensively used during the past two decades for the synthesis of V_2O_5 sol–gel nanocrystalline films [14–18]. V_2O_5 gels are easily made by the acidification of aqueous solutions of sodium metavanadate $NaVO_3$ through a proton-exchange resin. However, several other syntheses, such as the hydrolysis of vanadium oxo-alkoxide $VO(OR)_3$, the exothermic reaction of V_2O_5 with hydrogen peroxide, pouring V_2O_5 melt into water and even the very slow dissolution of V_2O_5 in pure water, have been reported in the literature [14, 15, 19]. In all cases, a clear yellow solution is first formed that progressively turns red while its viscosity increases. A dark-red sol–gel of the general composition $V_2O_5 \cdot nH_2O$ is obtained after a few minutes, hours or even months depending on the experimental procedure. It remains stable for years when kept in a closed vessel in order to prevent water evaporation [19].

Although $V_2O_5 \cdot nH_2O$ xerogel is known to be lamellar, with an interlayer distance of 1.15 nm, its actual structure remained an unresolved issue for some time. Livage and coworkers [21] proposed that the V_2O_5 layers are composed of corrugated single layers of VO_5 ribbons with a step of 0.28 nm, with the intra-ribbon structure being closely related to the layers of orthorhombic V_2O_5 (Fig. 1a). However, Oka and coworkers [22] proposed a different structure applying Rietveld analysis in which the layers consist of two V–O polyhedra sheets facing each other at a distance of 0.28 nm according to the structure of

AgV_2O_5 (Fig. 1b). The debate on the structural model comes out of the observed X-ray pattern of the gel. Actually, the observed $00l$ class of reflections is explained for both models in some detail by simple Patterson analysis [23]. Recently, depending on polarized X-ray absorption spectroscopy [24] and the pair distribution function (PDF) [25], the results of Oka's model are supported. In such a gel, V_2O_5 layers are formed by cross-linked fibers and are separated by water molecules [15]. While the interlayer spacing depends on the water content, it discontinuously decreases by a step of 0.28 nm when water is removed, as pointed out by Livage and coworkers applying an X-ray diffraction technique [21]. Sudden drops of the interlayer spacing from 1.155 nm to 0.875 nm have been reported for $\text{V}_2\text{O}_5 \cdot 1.6\text{H}_2\text{O}$ and $\text{V}_2\text{O}_5 \cdot 0.5\text{H}_2\text{O}$, respectively [21]. These results were interpreted as due to the existence of two different phases. The structure of the fibers themselves is not modified during the swelling process and can be presumably related to the lamellar structure of orthorhombic vanadium pentoxide.

Vanadium pentoxide xerogel, $\text{V}_2\text{O}_5 \cdot n\text{H}_2\text{O}$, films have been extensively studied because of many interesting properties. These sol–gel films can be used as reversible cathodes in lithium batteries, electrochromic layers for display devices, host materials for the intercalation of guest species, switching devices, gas sensors, high energy density lithium microbatteries or catalysts etc. [17]. Vanadium oxide gel is even a constituent of smart artificial muscle [20].

2 Experimental

In the present work vanadium pentoxide gel is formed by pouring 2 g V_2O_5 melt (800 °C) into 20 cm³ distilled water; this mixture was continuously stirred at a fixed temperature of 60 °C until condensation. A film was dip coated on a flat glass substrate specially shaped to match the X-ray diffractometer oven sample holder. The substrate glass material was so chosen in order not to affect our final thermal expansion results. A Na-borosilicate glass substrate with very small PTE within the present working conditions was used [26].

X-ray diffraction data at room temperature and above were obtained using a Shimadzu 6000 diffractometer, equipped with an oven (type HA-1001), which is capable of operating under normal ambient conditions and under vacuum [27]. The X-rays from a copper tube were monochromated with a graphite crystal to give monochromatic $K_{\alpha 1}$ radiation. A gas-filled proportional counter collects data over the range 4° to 60° in steps of 0.02°. Data were collected at different temperatures ranging from 23 to 180 °C in air. The total elapsed period due to fixing the sample temperature before data collection extended to about 20 min, i.e. the sample was in thermodynamic equilibrium with the environment. After cooling to room temperature, two extra exposures were done at room temperature in air and in vacuum of 2×10^{-2} Torr. The X-ray diffraction data evaluation was performed by the software ORIGIN 6 using a profile-fitting approach in order to extract the diffraction line positions. A pseudo-Voigt function was used to model the diffraction lines. The software ORIGIN 6 was also applied to extract the integrated peak area. Reference material was standard silicon, SRM 640C, specifically specified for 2θ calibration. The error in line position, $\Delta 2\theta$, never exceeds $\pm 0.015^\circ$. On the other hand, differential scanning calorimetry (DSC) analysis was carried out under nitrogen atmosphere up to 300 °C in a Shimadzu DSC-50 calorimeter. The heating rate was 10 °C/min. An infrared absorption spectrum was collected at room temperature using a conventional KBr pellet method on a Fourier transform infrared (FTIR) spectrometer (Perkin–Elmer 1760 X).

3 Results and discussion

Recently, in a study of the optical and electrical properties of a $\text{V}_2\text{O}_5 \cdot n\text{H}_2\text{O}$ gel film we observed an abnormal behavior below 100 °C during measurements of the electrical conductivity and the thermoelectric power in air [14]. This observation is a special property of the present V_2O_5 xerogel and is not related to VO_2 precipitation, as proved by the X-ray diffraction result as well as the electrical conductivity [14]. Accordingly, in the present work it was originally our aim to explore the origin of this abnormality by applying high-temperature X-ray diffraction in the temperature range from room temperature to 180 °C,

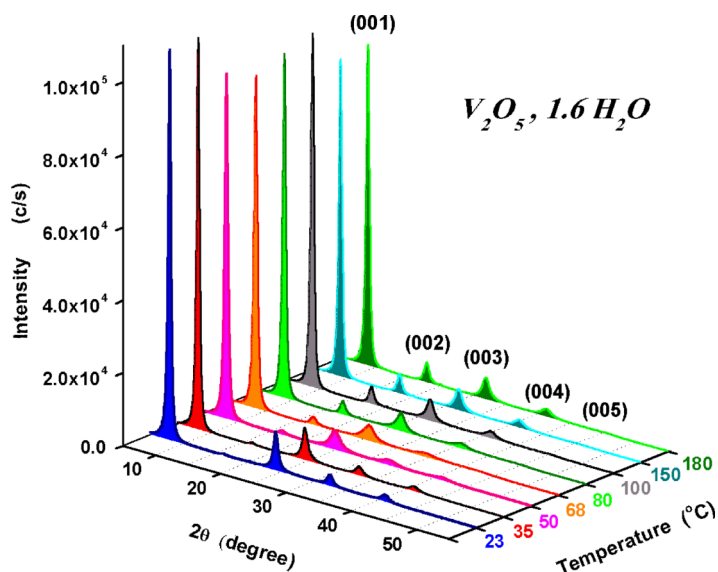


Fig. 2 (online colour at: www.pss-a.com) In-air X-ray diffraction of $V_2O_5 \cdot nH_2O$ xerogel as obtained in the present work at different temperatures.

without causing any phase change of the original film structure or crystalline growth. We were surprised to observe a continuous linear contraction of the lattice along the 001 reflections as well as its other entire harmonics, 002, 003, etc., in contradiction to earlier reports which pointed out that a *step* of 0.28 nm shrinkage is noticed as the temperature rises [15, 21]. Consequently, the main goal of the present work is now to report and discuss this behavior of a $V_2O_5 \cdot nH_2O$ xerogel film. To our knowledge this phenomenon has not been previously reported explicitly for this material [15]. The observed coefficient of NTE is found to be two orders of magnitude higher than any previously reported one for any material [4, 5, 7, 8, 10], as will be shown later. The mechanism that could explain this observed giant NTE behavior of a $V_2O_5 \cdot nH_2O$ sol–gel film will be briefly discussed on the basis of the extrinsic mechanism of dehydration.

Figure 2 shows present X-ray diffraction patterns for a vanadium pentoxide xerogel film measured at different temperatures. As shown, the xerogel film has a lamellar structure. However, it can be observed that the diffraction lines are shifted to higher angles as the temperature increases as shown in Fig. 3, where the position of the 001 diffraction peak changes from $2\theta (7.980 \pm 0.001)^\circ$ to $(8.899 \pm 0.001)^\circ$, i.e. $d(001)$ changes from 1.107 nm to 0.9929 nm at 23 °C and 180 °C, respectively. These values of $d(001)$ indicate that our sample may be presented as $V_2O_5 \cdot 1.6H_2O$ at room temperature assuming a linear variation of the interlayer spacing as given in [15] and stated above. Notice that the peaks corresponding to the diffraction harmonic 003 for example also have the same trend. However, as can be seen in Fig. 2, the amplitude of the 001 diffraction is much larger and thus in the following we will concentrate on the diffraction peak of the first harmonic from the 001 planes. It was also noted that although it shows the same NTE behavior, the diffraction peak area of the 002 planes increases as the temperature rises by about 28 times within the studied temperature interval (Fig. 4a and b). This behavior may be explained as due to the increase of the atomic structure factor as the interlayer water content is reduced continuously. Whereas the interlayer spacing contracts, the total effective number of electrons increases as the VO_5 ribbons of the two layers are approaching continuously. All diffraction lines, 001, 002, 003 etc., produced the same linear NTE coefficients of $-1.51 \times 10^{-3} K^{-1}$ and $-1.37 \times 10^{-4} K^{-1}$ in the temperature ranges 23–90 °C and 90–180 °C respectively, as shown graphically in Fig. 5. Values of the NTE coefficient are two orders of magnitude higher than any material reported in the literature [4, 5, 7]. This layered structure of the gel is to be related to the lamellar structure of orthorhombic V_2O_5 obtained after crystallization of the gel above 350 °C [21].

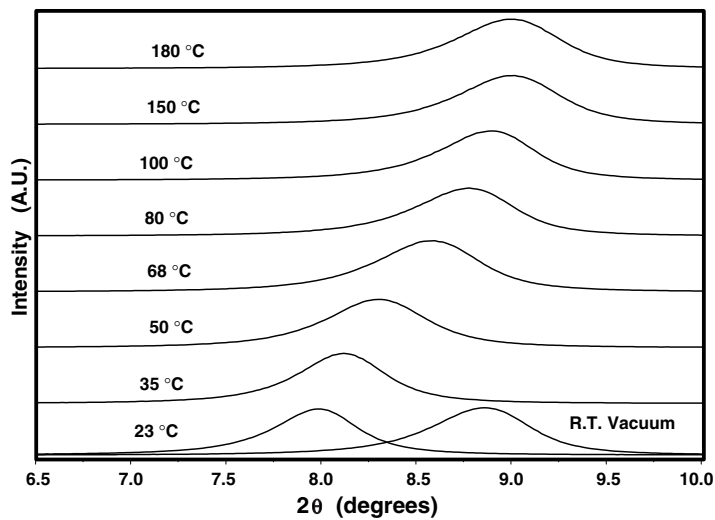


Fig. 3 In-air X-ray diffraction patterns for the 001 reflection at different temperatures, extracted from Fig. 1.

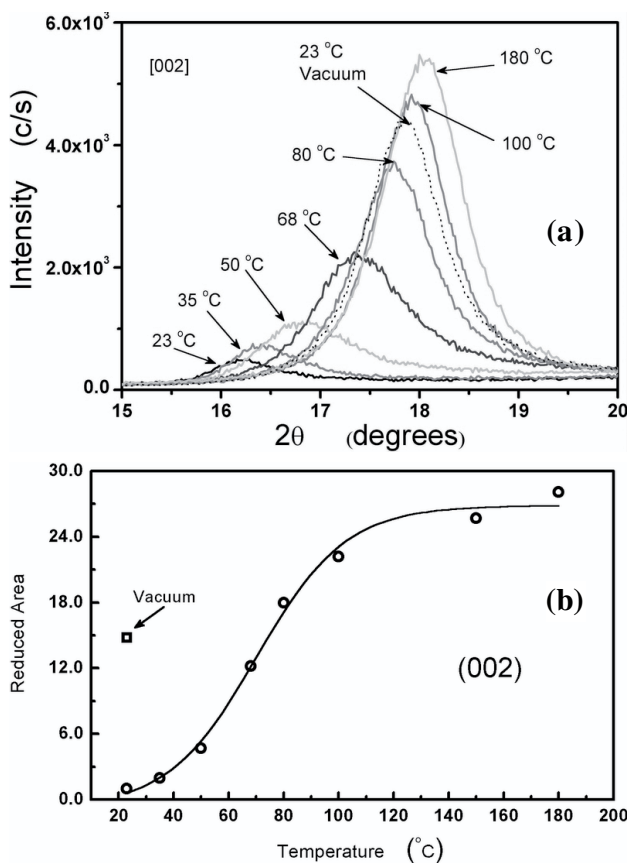


Fig. 4 a) Set of X-ray diffraction scans for the 002 reflection at different temperatures in air as indicated, extracted from Fig. 1, and showing the gradual shift to higher 2θ as the temperature is raised. b) Variation of the reduced total area (relative to the room-temperature area) of the 002 peak as a function of temperature. The data point \square represents the corresponding total area of the room-temperature run under vacuum.

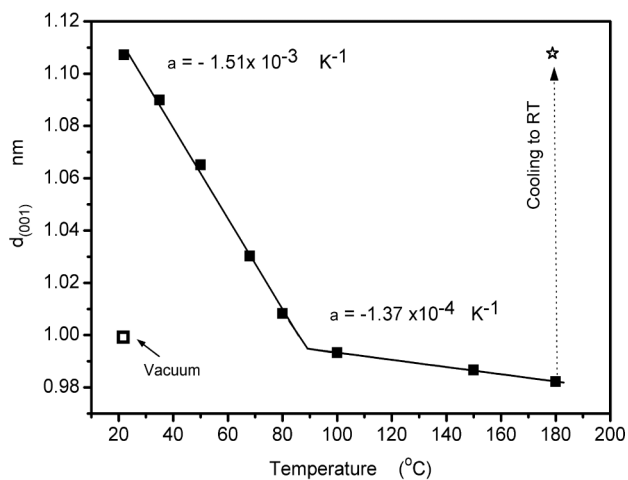


Fig. 5 Variation of the lattice spacing of the X-ray diffraction 001 reflection as a function of temperature. The open star, \star , represents the room-temperature measurement in air following cooling. The open square, \square , represents room-temperature measurements in vacuum following cooling.

As shown in Fig. 6, the present DSC thermogram shows mainly two endothermic peaks. The first unsymmetrical positively skewed low-temperature peak suggests a superposition of more than one endothermic reaction. Profile analysis indicates two endothermic reactions marked as I and II in Fig. 6. Accordingly, three stages of water release are seen on the DSC curve below 300 °C, see Fig. 6. The present DSC thermogram is similar to that reported in [21]. However, slight differences may be due to unlike methods of preparation. The origin of the water can be described as reported in [21]; mostly free water reversibly adsorbed interstitially between the V_2O_5 layers, I stage, a more strongly bonded water into the layers cross linking the fibers through hydrogen bonds, II stage, and a very small amount of water chemically bonded to vanadium, III stage as shown in Fig. 6, respectively. Upon heating, the weakly bonded water first goes below 90 °C and bottoms at 68 °C, decreasing gradually the interlayer spacing as clearly shown in Figs. 3 and 5, respectively. Another NTE coefficient was obtained after all the bonded water has been released above 90 °C (Figs. 5 and 6) and bottomed at 100 °C. The structural identity remains the same up to 180 °C without any phase change as shown in Fig. 2. Above 180 °C only the departure of

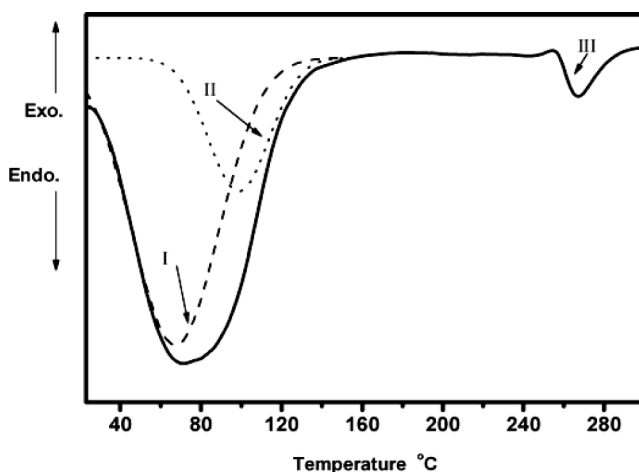


Fig. 6 DSC thermogram showing three different endothermic reactions, I, II and III, respectively, indicating three different stages of water dehydration as discussed in the text.

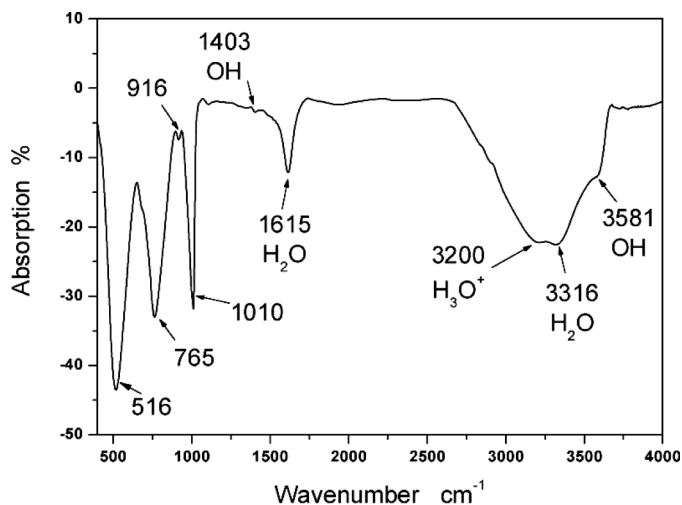


Fig. 7 Room-temperature FTIR spectrum of the $V_2O_5 \cdot nH_2O$ xerogel as obtained in the present work. IR absorption band positions of different structure groups are pointed out by arrows.

the chemically bonded water allows the rearrangement of these layers, leading to the crystallization of the oxide V_2O_5 above $300\text{ }^\circ\text{C}$ [22].

Consequently, it should be noted that the amount of water (e.g. H_2O , OH and/or H_3O^+ [10]) intercalation does not affect the structural identity of the V_2O_5 framework as confirmed by X-ray diffraction, where only a linear contraction of the c -axis is observed. Full recovery of the interlayer spacing is obtained after cooling the sample to room temperature in open air, see Fig. 5, where water molecules are reabsorbed upon cooling, indicating that the process is reversible and the heating process can be repeated without losing the NTE properties. Furthermore, it can be noted that the loosely bonded water can be eliminated by keeping the sample under vacuum. This is clearly presented in Figs. 4b and 5 by the square, \square , data point.

In order to identify different structure groups, the absorption bands in the FTIR spectrum are marked as shown in Fig. 7 according to [10, 28]. The band at 516 cm^{-1} is characteristic of the stretching vibration of the $V-O_2$ bond, while the bands at 765 cm^{-1} and 916 cm^{-1} may be assigned to VO_4 tetrahedra and VO_5 pyramid bond stretching. The band at 1010 cm^{-1} may be attributed to the stretching mode related to the shortest vanadium–oxygen bond $V=O$ [28]. On the other hand, different water species are marked according to [10], where absorption bands of the stretching vibration modes (between 3100 and 3650 cm^{-1}) and deformation vibration modes (between 1400 and 1650 cm^{-1}) of H_2O , H_3O^+ and OH species are indexed as shown in Fig. 7.

4 Conclusion

In conclusion, we have shown that vanadium pentoxide gels, $V_2O_5 \cdot 1.6H_2O$, give rise to xerogel layers that exhibit a preferred orientation. X-ray diffraction of this xerogel displays the $00l$ peaks typical of a turbostratic [25] stacking of the V_2O_5 ribbons along a direction parallel to the substrate. Water molecules are intercalated between the ribbons and the distance along the c -axis decreases linearly as the temperature is raised to $180\text{ }^\circ\text{C}$, as observed by high-temperature X-ray diffraction. This contraction is associated with progressive dehydration and is thus due to an extrinsic mechanism of negative thermal expansion, NTE. The coefficient of NTE as large as $-1.5 \times 10^{-3}\text{ K}^{-1}$ was observed. Full recovery of the interlayer spacing is obtained after cooling the sample to room temperature in open air, where water molecules are reabsorbed, indicating that the process is reversible and the heating process can be repeated without losing NTE. A further study of the nature of the water species, e.g. H_2O , OH and/or H_3O^+ , is under way.

References

- [1] A. W. Sleight, *Nature* **425**, 674 (2003).
- [2] R. W. Cahn, *Nature* **386**, 22 (1997).
- [3] A. W. Sleight, *Curr. Opin. Solid State Mater. Sci.* **3**, 128 (1998).
- [4] P. M. Jardim, B. A. Marinkovic, A. Saavedra, L. Y. Lau, C. Baetz, and F. Rizzo, *Microporous Mesoporous Mater.* **76**, 23 (2004).
- [5] G. D. Barrera, J. A. O. Bruno, T. H. K. Barron, and N. L. Allan, *J. Phys.: Condens. Matter* **17**, R216 (2005).
- [6] J. S. O. Evans, T. A. Mary, T. Vogt, M. A. Subramanian, and A. W. Sleight, *Chem. Mater.* **8**, 2809 (1996).
- [7] S. Sumithra and A. M. Umarji, *Mater. Res. Bull.* **40**, 167 (2005).
- [8] M. P. Attfield and A. W. Sleight, *Chem. Mater.* **10**, 2013 (1998).
- [9] D. A. Woodcock, P. Lightfoot, L. A. Villaescusa, M. Diaz-Caban, M. A. Cambor, and D. Engberg, *Chem. Mater.* **11**, 2508 (1999).
- [10] B. A. Marinkovic, P. M. Jardim, A. Saavedra, L. Y. Lau, C. Baetz, R. R. de Avillez, and F. Rizzo, *Microporous Mesoporous Mater.* **71**, 117 (2004).
- [11] J. R. Salvador, F. Guo, T. Hogan, and M. G. Kanatzidis, *Nature* **425**, 702 (2003).
- [12] B. De Meyer, L. Vandeperre, I. Van Driessche, E. Bruneel, and S. Hoste, *Cryst. Eng.* **5**, 469 (2002).
- [13] J. Livage, *Catal. Today* **41**, 3 (1998).
- [14] A. A. Bahgat, F. A. Ibrahim, and M. M. El-Desoky, *Thin Solid Films* **489**, 68 (2005).
- [15] J. Livage, *Coord. Chem. Rev.* **190–192**, 391 (1999); *Coord. Chem. Rev.* **178–180**, 999 (1998).
- [16] C. Sanchez, J. Livage, J. P. Audiere, and A. Madi, *J. Non-Cryst. Solids* **65**, 285 (1984).
- [17] J. Livage, *Solid State Ion.* **86–88**, 935 (1996).
- [18] J. Livage, *J. Chem. Mater.* **3**, 578 (1991).
- [19] J. Livage, O. Pelletier, and P. Davidson, *J. Sol–Gel Sci. Technol.* **19**, 275 (2000).
- [20] J. Livage, *Nat. Mater.* **2**, 297 (2003).
G. Gu, M. Schmid, P. Chiu, A. Minett, J. Frayssé, G. Kim, S. Roth, M. Kozlov, E. Muñoz, and R. H. Aughman, *Nat. Mater.* **2**, 316 (2003).
- [21] P. Aldebert, N. Baffier, N. Gharbi, and J. Livage, *Mater. Res. Bull.* **16**, 669 (1981).
- [22] T. Yao, Y. Oka, and N. Yamamoto, *Mater. Res. Bull.* **27**, 669 (1992).
- [23] Y.-J. Liu, J. L. Schindler, D. C. DeGroot, C. R. Kannewurf, W. Hirpo, and M. G. Kanatzidis, *Chem. Mater.* **8**, 525 (1996).
- [24] M. Giorgetti, S. Passerine, W. H. Smyrl, and M. Berrettoni, *Inorg. Chem.* **39**, 1514 (2000).
- [25] V. Petkov, P. N. Trikalitis, E. S. Bozin, S. J. L. Billinge, T. Vogt, and M. G. Kanatzidis, *J. Am. Chem. Soc.* **124**, 10157 (2002).
- [26] M. M. Lima and R. Monteiro, *Thermochim. Acta* **373**, 69 (2001).
- [27] S. Al-Henitia and A. Al-Hajry, *J. Alloys Compd.* **387**, L5 (2005).
- [28] Z. V. Popovic, M. J. Konstantinovic, R. Gajic, V. N. Popov, M. Isobe, Y. Ueda, and V. V. Moshchalkov, *Phys. Rev. B* **65**, 184303 (2002).